

COMPACT SUPPORT RADIAL BASIS FUNCTIONS FOR SOFT TISSUE DEFORMATION

Mark P. Wachowiak¹, Xiaogang Wang¹, Aaron Fenster^{1,2}, Terry M. Peters^{1,2}

¹Robarts Research Institute, London, ON CANADA

²University of Western Ontario, London, ON CANADA

ABSTRACT

We describe the use of compact support radial basis functions (CSRBFs) for simulation of soft tissue deformation. CSRBFs allow surface and volumetric deformations to be computed in near real time. In comparison to other spline functions, CSRBFs effect local deformations. In addition, CSRBF matrices are guaranteed to be positive definite and invertible. Visual realism can be achieved by utilizing different CSRBFs with deformation behaviour approximating specific soft tissue characteristics, and by a locality parameter. Computations can also be performed in parallel for increased efficiency. The efficacy of this deformation model is demonstrated on data from a 3D prostate image for the application of needle insertion for implanting radioactive seeds for brachytherapy.

1. INTRODUCTION

Most current research into surgery simulation and soft-tissue modeling utilizes biomechanical models, such as finite element and mass-spring paradigms. These models provide a high degree of physical realism, and can also be used to study tissue and organ properties. However, they are very computationally intensive, and, as yet, are not conducive to real-time simulation (at least 15 frames per second display refresh rate). For many applications where high-frame rates and visual realism are required, such as surgical simulation and training, absolutely realistic deformation modeling is not always required, and non-physical deformation models may be sufficient [1]. The ChainMail [2,3] and sphere-filled models [4], which rely on physical analogies but do not directly incorporate biomechanical parameters, can achieve real-time performance in many cases. Additionally, superquadrics incorporate motion and stiffness parameters for increased physical realism [5]. Like splines [6], compact support radial basis functions

(CSRBFs) model deformations by interpolating displacements between source and target points. However, CSRBFs have the advantage that their effect is local, as opposed to thin-plate splines or multiquadratics. Locality is controlled with a scaling parameter. Deformation behaviour can be adjusted by utilizing different CSRBFs and by adjusting the scaling parameter. CSRBFs and spline functions have been applied to nonrigid registration [6,7]. CSRBFs have also been used in computer animation techniques [8]. However, in this case, deformation was computed only on surface points. In the current study, volumetric deformation is achieved by displacing both points on the surface within the volume.

2. COMPACT SUPPORT RBFS

2.1 Theory

Let \mathbf{p} and \mathbf{q} respectively denote a set of n source and target landmarks. The displacements u for points \mathbf{x} are:

$$u(\mathbf{p}_i) = \mathbf{q}_i, u(\mathbf{x}) = \phi(\mathbf{x}) + \sum_i \alpha_i R(\|\mathbf{x} - \mathbf{p}_i\|), i = 1, \dots, n \quad (1)$$

where $\phi(\bullet)$ is a linear combination of polynomials and $R(\bullet)$ denotes a RBF. Let \mathbf{K} denote the $n \times n$ matrix given by $\mathbf{K}_{i,j} = R(\|\mathbf{p}_i - \mathbf{p}_j\|)$. For any CSRBF, R , \mathbf{K} is positive definite, and therefore no polynomial term ϕ is required [7]. \mathbf{K} is also guaranteed to have an inverse. Thus, the coefficients α are solved by $\alpha = \mathbf{K}^{-1}\mathbf{q}$.

Two important classes of CSRBFs are Wendland functions, constructed from piecewise polynomials [9], and a general class of functions, introduced by Buhmann, that includes the Wendland CSRBFs as special cases [10]. For a specified dimension $d > 0$ and smoothness parameter $k \geq 0$ there exists a unique Wendland function, $\psi_{d,k}(r) \in C^{2k}(\mathfrak{R})$ which is positive definite on \mathfrak{R}^d and has a polynomial of minimal degree $\text{floor}(d/2) + 3k + 1$. Three examples of such functions for $d = 3$ are given as [9]:

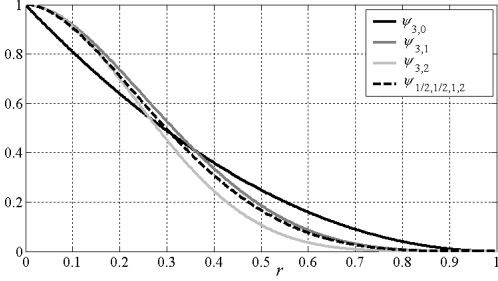


Figure 1. Examples of Wendland and Buhmann CSRBFs.

$$\psi_{3,0}(r) = (1-r)_+^2, \quad \psi_{3,1}(r) = (1-r)_+^4(4r+1),$$

and $\psi_{3,2}(r) = (1-r)_+^6(35/3r^2 + 6r + 1),$ (2)

where $(1-r)_+^l = (1-r)^l$ for $0 \leq r \leq 1$ and 0 otherwise. In addition to the dimension, the Buhmann functions are parameterized by four numbers [10]. An example of a 3D Buhmann CSRBF with parameters $\frac{1}{2}, \frac{1}{2}, 1,$ and 2 is [10]:

$$\psi_{3,1/2,1/2,1,2}(r) = 12r^4 \ln(r) - 21r^4 + 32r^3 - 12r^2 + 1 \quad (3)$$

where $0 \leq r \leq 1$ and $\psi(0) \equiv 0$. Plots of these functions are shown in Figure 1.

2.2 CSRBFs in soft tissue deformation

Behaviour of CSRBFs are controlled by locality and the choice of the specific function, with smoother, more nonlinear deformations provided with $k > 0$. The global effect of ψ increases with a spatial support parameter, $a > 0$. The CSRBF is scaled as $\psi_a(r) \equiv \psi(r/a)$, and its mathematical properties are not affected [7].

In surgery simulation, under the assumption of a rigid surgical instrument, the position of the tip of the instrument with the tissue during the first collision is the source landmark. The target landmark is the new position of the tip of the instrument after pressure application. For simple instruments, such as needles, one landmark is sufficient. The number of landmarks increases with the area of contact between the instrument and tissue. In terms of Eq. (1), \mathbf{p} is the set of positions of the instrument/tissue contact points and any internal landmarks, and \mathbf{q} is the set of displaced instrument contact positions and those of internal landmarks.

Tissue stiffness can be simulated with anchor landmarks placed inside the tissue or organ. If the source and target internal landmarks are identical, displacements around these points are restricted. Anchor landmarks can be placed close to the surface to simulate stiff material, while landmarks placed in more interior locations allow deeper deformations. The distance of the interior

landmarks from the surface may also change dynamically in response to stimuli, and to simulate stiff homogeneous material. A simple, automated method to place interior landmarks in mostly convex objects is to compute the centroid of surface coordinates, and scale a small subset of the surface points by a scale factor $\lambda < 1$ about the centroid.

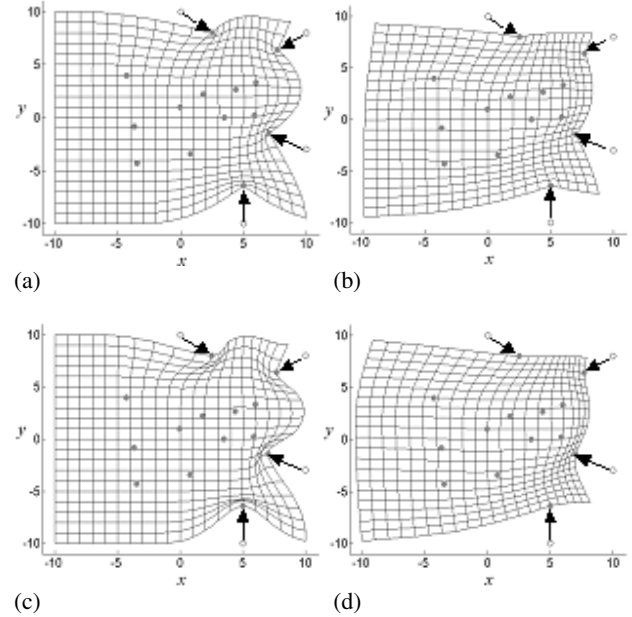


Figure 2. 2D grid deformation with CSRBFs and 10 interior landmarks. (a) $\psi_{3,0}, a = 8$. (b) $\psi_{3,0}, a = 40$. (c) $\psi_{3,2}, a = 8$. (d) $\psi_{3,2}, a = 40$.

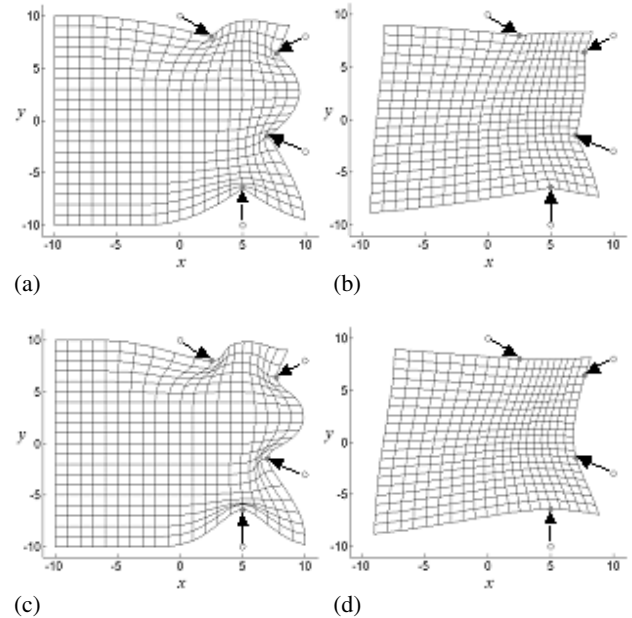


Figure 3. Deformation with CSRBFs, no interior landmarks. (a) $\psi_{3,0}, a = 8$. (b) $\psi_{3,0}, a = 40$. (c) $\psi_{3,2}, a = 8$. (d) $\psi_{3,2}, a = 40$.

For dynamic behavior, λ can be allowed to decrease when pressure is applied to the object, and to increase as pressure decreases. This approach is illustrated in the 2D case in Figure 2, where ten internal landmarks are placed within a 2D mesh, and pressure is applied at four locations. In Figure 3, the same deformations are applied without utilizing anchor landmarks.

3. APPLICATION TO NEEDLE INSERTION SIMULATION IN PROSTATE BRACHYTHErapy

The efficacy of using CSRBFs for soft tissue deformation simulation was tested on prostate data, within prostate brachytherapy simulation framework [3]. In real-time transrectal ultrasound-guided brachytherapy, radioactive seeds are implanted into the prostate according to a patient-specific dosage plan. Because it is minimally invasive, interest in this technique is increasing. A critical factor in the success of this procedure is accurate seed delivery based on a dosimetric plan that maximizes destruction of the cancerous cells, while minimizing damaging to healthy tissue.

The online simulation involves an interactive visual simulation, haptic feedback, and TCP/IP based communication [3]. The soft tissue model, a volumetric prostate, was generated from a pre-operative 3D ultrasound volume and its segmented boundary. The model consists of 14,560 points, including 1,200 on the surface. Two bandwidths were set for the visual simulation: 30Hz for graphical rendering, and 200Hz for deformation computations and user interaction. The simulation currently runs on a 2.1 GHz personal computer. Using a simple collision detection algorithm [3], the landmark corresponding to the contact point between the needle tip and the tissue was identified.

4. RESULTS

The deformations caused by needle insertion are shown in Figure 4 for $\psi_{3,0}$ and $\psi_{3,1}$. Eight internal landmarks were selected randomly from the surface points scaled by $\lambda = 0.5$ about the centroid. From the figures, it can be seen that $\psi_{3,0}$ simulates deformation of more elastic material, while $\psi_{3,1}$ simulates stiffer material. The locality parameter a is an indicator of hardness, with low a indicating a greater degree of locality, and therefore harder material. The localized behaviours shown in Figs. 4c and 4d are indicative of the expected deformation with this specific tissue, but validation using real tissue properties is required. A surface representation of the same data, deformed with $\psi_{3,0}$ and $\psi_{3,1}$, is shown in Figure 5.

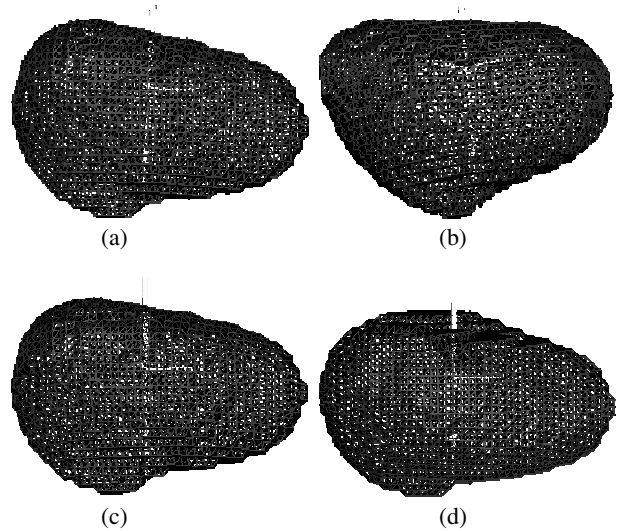


Figure 4. Mesh representation of prostate data (8 internal landmarks) after needle insertion. (a) $\psi_{3,0}$ with $a = 12$. (b) $\psi_{3,1}$, $a = 12$. (c) $\psi_{3,0}$ with $a = 6$. (d) $\psi_{3,1}$, $a = 6$.

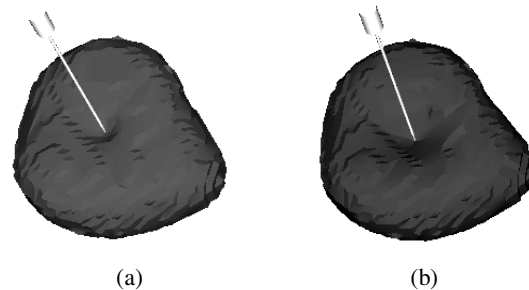


Figure 5. Surface rendering of prostate data after needle insertion. (a) Deformation with 8 internal landmarks using $\psi_{3,0}$ with $a = 6$. (b) No internal landmarks, using $\psi_{3,1}$ with $a = 12$.

5. DISCUSSION

At present, the most realistic deformations are attained with finite element, mass spring, and other physically-based models. However, new classes of meshfree and hybrid methods are increasingly studied because they require less preprocessing time, and, in some cases, they may be solved more efficiently [11, 12]. In some of these paradigms, spline and RBFs are used directly in finite element models [11]. In particular, CSRBFs are now applied to 3D physical problems that were formerly solvable only with finite elements [13].

Soft tissue deformation with CSRBFs can achieve visual realism at frame rates necessary for interactive simulation. The Wendland functions are polynomials, and do not require evaluation of roots or of transcendental functions (as do other splines) or trigonometric functions (superquadrics). Additionally, depending on the distribution of landmarks, for small a ,

the \mathbf{K} matrix is generally sparse [5], and the inverse can be computed with specialized methods. Because a polynomial component ϕ is not required, \mathbf{K} has size $n \times n$, and the coefficients α can be efficiently determined. Efficiency greatly depends on the number of landmarks used, as the size of \mathbf{K} increases quadratically with n . For a small number of landmarks ($n \leq 10$), near real time performance, about 25 computations per second, can be achieved for the Wendland functions, as shown in Figure 6a (in this case, the displacements of all 14,560 points of the prostate data were computed). The Buhmann CSRBF, Eq. (3), contains a logarithm term and is more complex. Solving for α and computing displacements are inherently parallel, and efficiency can be further increased if multiple processors are available. Figure 6b shows the timing results of parallelizing the computations with four processors and shared memory (implemented with OpenMP). Efficiency greatly increases for all CSRBFs. Near real time computations can be performed with 30 and 20 landmarks using Wendland and Buhmann CSRBFs, respectively.

In this study, landmarks represent the interface between the instrument and tissue, and are also constraints that allow simulation of tissue hardness, assuming primarily homogeneous material. Heterogeneous tissue may be simulated by allowing a to assume different values for each landmark. However, the internal landmarks must be chosen very carefully. In addition, the invertibility of \mathbf{K} can no longer be guaranteed theoretically, although such an approach was successfully applied to nonlinear image registration [7].

6. CONCLUSION

This paper demonstrates the efficacy of using compact support radial basis functions for simulating soft tissue deformation. The CSRBF model was applied to simulation of needle insertion for prostate brachytherapy. Real time frame rates and visual realism were attained with appropriate selection of basis functions, locality parameters, and internal landmarks. The efficiency of the CSRBF can be improved with parallelization.

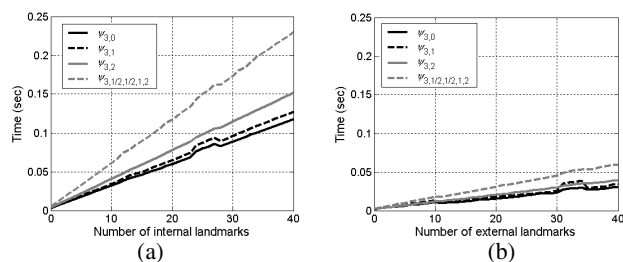


Figure 6. Computation time for 14,560 displacements using CSRBFs. (a) One processor (1.0 GHz Compaq/HP® ES45™). (b) Four processors on the same architecture, shared memory.

The CSRBF model, like all basis function approaches, has limitations. Its primary use is deformation, and actions that change topology, such as cutting, are difficult to simulate. The method also assumes relatively homogeneous tissue and concave geometry. Choice of parameters is empirical. Thus, future work will focus on incorporating CSRBFs into physics-based modeling paradigms, adding elasticity properties, on developing a framework for parameter selection, and on validation.

7. REFERENCES

- [1] A. Liu, F. Tendick, K. Cleary, and C. Kaufmann, "Medical Simulation for Surgical Training," *MICCAI (Tutorial)*, 2001.
- [2] S. F. F. Gibson, "Using Linked Volumes to Model Object Collisions, Deformation, Cutting, Carving, And Jointing," *IEEE Trans. on Visual. & Comp. Graph.* **5**, pp.333-348, 1999.
- [3] X. Wang and A. Fenster, "Haptic-Enhanced 3D Real-Time Interactive Needle Insertion Simulation System for Prostate Brachytherapy," To appear in *Proc. SPIE Med. Imag.*, 2004.
- [4] N. Suzuki and D. Suzuki, "Surgery Simulation System with Haptic Sensation and Modeling of Elastic Organ That Reflect the Patients' Anatomy", *Proc. Surgical Simulation and Soft Tissue Modeling*, pp. 155-164, 2003.
- [5] D. Terzopoulos and D. Metaxas, "Dynamic 3D Models with Local and Global Deformations: Deformable Superquadrics," *IEEE Trans. Patt. Anal. Mach. Intel.* **13**, pp. 703-714, 1991.
- [6] D. G. Gobbi and T.M. Peters, "Generalized 3D Nonlinear Transformations for Medical Imaging: An Object-Oriented Implementation in VTK," *Comp. Med. Imag. Graphics* **27**, pp. 255-265, 2003.
- [7] M. Fornefett, K. Rohr, and H. S. Stiehl, "Radial Basis Functions with Compact Support for Elastic Registration of Medical Images", *Image Vision Comput.* **19**, pp. 87-96, 2001.
- [8] N. Kojekine, V. Savchenko, M. Senin, and I. Hagiwara, "Real-time 3D Deformations by Means of Compactly Supported Radial Basis Functions," *Eurographics 2002*, Ed. I. N. Alvaro and Ph. Slusallek, 2002.
- [9] H. Wendland, "Piecewise Polynomial, Positive Definite and Compactly Supported Radial Functions of Minimal Degree," *Adv. in Comp. Math.* **4**, pp. 389-396, 1995.
- [10] M.D. Buhmann, "A New Class of Radial Basis Functions with Compact Support", *Math. Comput.* **70**, pp. 307-318, 2000.
- [11] G. R. Liu, *Mesh Free Methods: Moving Beyond the Finite Element Method*, CRC Press, Boca Raton, FL, 2002.
- [12] K. Höllig, *Finite Element Methods with B-Splines*, SIAM Press, Philadelphia, PA, 2003.
- [13] C.S. Chen, M. Marcozzi, and S. Choi, *The Method Of Fundamental Solutions and Compactly Supported Radial Basis Functions - A Meshless Approach in 3D Problems*, Boundary Element Methods XXI, Ed. C.A. Brebbia and H. Power, WIT Press, Boston, pp. 561-570, 1999.

ACKNOWLEDGEMENTS

Funding for this project was provided by SHARCNet, NSERC (R3146-A02), CIHR (MT 14735), (MT 11540), and (MGP 49536). Thanks is given to Ravi Gupta for technical assistance.